ANGLE-DEPENDENT CHARGE FRACTION OF 16 MEV ^{16}O IONS AFTER PASSING THROUGH THIN CARBON FOILS

Sakamoto, H. Ogawa. and N. Shiomi-Tsuda.
Department of Physics, Nara Women's University, Nara 630, Japan

Abstract

Charge fractions of 16 MeV ^{16}O ions which passed through thin carbon foils were measured as a function of emergence angle. The thickness of carbon foils used in the present experiment ranged from 1,9 to 52,1 $\mu g/cm^2$. Observed charge fractions of 4+, 5+, 6+, 7+ and 8+ states were roughly 6%, 27%, 51%, 15% and 1%, respectively. Depending on their charge states, charge fractions of emerging ^{16}O ions were found to increase or decrease with increasing emergence angle. Using computer simulations with total cross sections for chargechanging collisions, we could reproduced measured charge fractions reasonably well. The charge state equilibrium was shown to be attained at the target thickness of about 7 $\mu g/cm^2$. Even for a carbon target of 52,1 $\mu g/cm^2$, which was more than seven times thicker than 7 $\mu g/cm^2$, observed charge fractions of 4+ and 5+ states decreased and those of 7+ and 8+ states increased with increasing emergence angle.

I. Introduction

Equilibrium charge fractions and charge distribution widths of various ions after passing through matter have been studied experimentally and theoretically for a long time by many authors and lots of data have been accumulated [1,2]. As for a carbon target, there exists a task work performed by Shima et al. [3] in which we can find many experimental data for various ions in a wide energy region. On the basis of our knowledge on atomic collision processes, the charge fractions of ions are expected to depend strongly on their emerging angle from thin solid targets. Unfortunately, at present we do not have enough knowledge on such a phenomenon.

On the other hand energy losses of ions have been found to increase with increasing their emergence angles from various targets [4-7]. The origin of this phenomenon is considered to be the impact parameter dependence of energy loss of ions in individual collisions which ions undergo within the target materials. From the microscopic standpoint of view, cross sections for charge-changing collisions should depend on scattering angles or on equivalent impact parameters. Accordingly, it is quite natural to anticipate that charge fractions are dependent on emerging angles as far as the target material is thin. Up to now it was well known that fractions of high charge states increase at large angles after a single charge-changing collision [8]. Moreover, in the recent experiment single- and double-electron capture probabilities of He^{2+} ions in large-angle scattering on Ar and N_2 targets were measured by Ben-ltzhak et al. [9]. They found that charge fractions varied depending on the impact parameter at large impact parameters but did not depend on it once the K-shell radius was crossed by projectiles.

In this paper we report experimental results on the angle-dependent charge fractions of 16 MeV ^{16}O ions after passing through thin carbon foils. Using total cross sections for charge-changing collisions, we performed computer simulations to obtain charge state distri butions. We will compare calculated charge fractions with measured ones. From the results of simulations we found that the charge state equilibrium was attained at the thickness of about 7 $\mu g/cm^2$. Even for much thicker targets than 7 $\mu g/cm^2$, charge fractions were ob served to vary with increasing emergence angle.

2. Experimental procedure

The schematic diagram of the experimental setup is shown in fig. I. The beam of 16 MeV ^{16}O ions from the 8MV tandem Van de Graaff accelerator of Kyoto University was collimated by a double diaphragm system of S1 and S2; the diameter of each was 0,7 mm and they were 193 cm apart. The angular divergence of the incident beam was thus less than 0.02° before hitting a carbon target. The ^{16}O ion beam of 4+ state was used in the present experiment. A baffle S3 of 1.5 mm diameter was placed 135 mm behind the diaphragm S2 in order to prevent the edge-scattered ^{16}O ions that originated at diaphragms S1 and S2 from entering a detector and affecting the charge fraction measurement. Self-supporting carbon targets were mounted 11 mm behind the baffle S3. A horizontal slit was placed 22 cm behind the target in order to permit only ^{16}O ions that were scattered by target atoms in the horizontal plane to go through it. A pair of permanent magnets, the magnetic field of which was about 1700 Gauss, were mounted after the horizontal slit. ^{16}O ions of various charge states were split vertically by these magnets and detected by a position sensitive detector (PSD) which was placed 118 cm behind the target. The detecting system, which consisted of a vertical slit and the PSD, was movable perpendicular to the incident beam direction in a range of a few cm. The displacement of 10 mm corresponds to the emergence angle of 0.49°.

The carbon foils of various thicknesses were commercially obtained and their mass thicknesses were determined by using the Rutherford backscattering method with 2.0 MeV alpha particles from the 1.7 MV tandem Van de Graaff accelerator at Nara Women's University. Hereafter we will use simply a word "thickness" in the meaning of mass thickness. The thicknesses of carbon targets used in the present experiment were 1.9, 3.0, 3.2, 8.0, 12.6, 26.1 and 52.1 $\mu g/cm^2$. Uncertainty of their thicknesses was estimated to be within ±5%.

The energy and position pulses from the PSD were amplified with standard amplifier systems and fed into a PSD analyzer (ORTEC 464). The output pulses of the PSD analyzer were recorded on a 2048-channel pulse height analyzer. Typical pulse height spectra obtained at emergence angles of 0° and 0.49° are shown in fig. 2.

3. Results

Charge fractions of 16 MeV ^{16}O ions after passing through carbon targets of 1.9, 8.0, 26.1 and 52.1 $\mu g/cm^2$ are shown in fig. 3. As was clearly seen in figs. 2 and 3, charge fractions of ^{16}O ions were found to vary with emerging angles. Charge fractions observed were roughly 6%, 27%, 51%, 15% and 1% for 4+, 5+, 6+, 7+ and 8+ states, respectively. The fraction of 3+ state was less than 1% and could be neglected in the later discussion because it did not play an important role in the charge state distribution and further because we could not obtain reliable data over the whole angles measured owing to its poor statistics. In any case, 6+ state has the largest fraction and we can suppose that the mean charge is around 6. The fraction of 6+ state shows rather weak dependence on emerging angles. The fractions of 4+ and 5+ states decrease with increasing emergence angle, while those of 7+ and 8+ states increase with emergence angle.

In the thinnest case of the 1.9 $\mu g/cm^2$ carbon target, fractions of 4+ and 5+ states are larger than those of 8+ and 7+ states, respectively, at all angles measured. In thicker target cases, however, fractions of 7+ and 8+ states exceed respectively those of 5+ and 4+ states at large angles. Little difference is observed in the angular dependence of charge fractions measured for carbon targets which are thicker than 8.0 $\mu g/cm^2$. Although in the thickest case of 52.1 $\mu g/cm^2$ carbon target the charge fraction of 6+ state shows a weak dependence on the emergence angle, it is interesting to noted that quite similar behaviors are observed in the angle-dependent charge fractions for thicker targets.

4. Computer simulation

To perform computer simulations, we need proper knowledge of cross sections for chargechanging collision processes. Since we have presently very little information on differential cross sections for these processes, simulations which we can carry out are restricted to those that treat total cross sections. Charge-changing cross sections have been measured mainly for gaseous targets. From these data systematic behaviors of cross sections were found for electron-capture and -loss processes.

Let us begin with single-electron capture cross sections because the scaling law of Knudsen et al. [10] was quite successful in giving a reasonable fit to existing experimental data. Fig. 4 shows the comparison of cross sections calculated by the scaling law with experimen tal data which were obtained by Boman et al. for 16 MeV ^{16}O ions [11]. One can find that experimental data are described very well by the scaling law. We will, therefore, use single-electron capture cross sections calculated by this scaling law in the present simulation.

As for single-electron loss cross sections, we do not have such a good scaling rule at hand nor a theoretical method which can reproduce measured cross sections reasonably well. Accordingly, we will estimate cross sections by relying on empirical formulas which were found by Baman et al. for 16 MeV ^{16}O ions of 5+, 6+ and 7+ states [11]. For projectiles of other charge states, cross sections were estimated on the basis of the independent-electron approximation (IEA) which predicted cross sections proportional to N. Here N stands for the number of "equivalent" L-shell electrons which incident ions carries. In the case of 19 MeV ^{19}F ions bombarding Ne and Ar atoms, the IEA was found to give reasonably good fits to measured cross sections [12].

In order to perform a realistic simulation, we should take into account double-electron transfer processes in addition to single-electron transfer processes because cross sections of such processes are not so small comparing with those of single-electron transfer processes. Although experimental data for double-electron capture and loss cross sections were rather scarce, it was found that the IEA was useful to estimate both double-electron capture and loss cross sections with a limited accuracy. For the estimation of double-electron capture cross sections, a scahng law that .cross sections are proportional to q^6 is also effective on the basis of the IEA and the scaling law of Knudsen et al., where q denotes the projectile charge. We used this scaling law and the experimental finding that $\sigma_{8,6} / \sigma_{8,7} \cong 0.1 - 0.2$ [12,13] to estimate cross sections. Here first and second subscripts indicate ion charges before and after charge-changing collisions, respectively. On the other hand, cross sections for double- electron loss processes are expected to be proportional to N(N- 1)/2 on the basis of the IEA as far as L-shell electrons are concerned. Cross sections are considered to be much smaller if K-shell electrons take part in the electron-loss processes because the binding energy of K-shell electrons is larger than that of L-shell electrons. We estimated double-electron loss cross sections assuming the validity of the IEA and also relying the experimental finding that $\sigma_{2,4} / \sigma_{2,3} \cong 0.4$ [12,13]. If K-shell electrons participate in the loss processes, we assumed one order of magnitude smaller cross sections for each K-shell electron.

Two sets of cross sections, which are hereafter referred as a set A and a set B, were used in the present simulation. In the set A, cross sections are estimated by the methods described above and no adjusting procedure is employed to fit experimental data. In the set B, cross sections obtained in the set A are slightly modified so that cross sections can reproduce a charge state distribution measured for 12.6 $\mu g/cm^2$ carbon target at 0°. The reasons why we prefered this distribution as the one that should be reproduced by a simulation are following. Firstly, from the rough estimation of charge-changing cross sections we can expect that the charge state equilibrium should be attained for a carbon target which is thicker than 10 $\mu g/cm^2$. Secondly, if

we rely on the theoretical estimation of angular distributions due to multiple scattering [14], the half width at half maximum for a 12.6 μg/cm^2 carbon target is less than 0.01°. Consequently, it is quite natural to consider that the charge state distribution observed when we measure all emerging ions is almost the same as that measured at 0°.

The evaluation methods of cross sections used in the present simulations are summarized in table I. Multi-electron transfer processes in which more than two electrons transfer to or from a projectile are neglected. The energy dependence of cross sections is also neglected because the energy loss of ^{16}O ions in carbon targets is small. ^{16}O ions lose about 3% of their initial energy when they passed through the thickest target used in this experiment.

Once a set of cross sections and a charge state of incident ions are given, calculations are rather straightforward. The procedure is as follows. In the first step, a mean free path for charge-changing collisions between an ^{16}O ion of a given charge and a carbon atom is calculated from cross sections for individual, charge-changing processes. In the second step, using the mean free path, the depth where a charge-changing colhsion takes place is calculated. When the depth exceeds the target thickness, the charge state of an ion is registered and a calculation is restarted for a new projectile. If the depth is smaller than the target thickness, a calculation proceeds next step. In the third step, an ion charge after the collision is calculated and then a computation continues returning to the first step. Charge state fractions are obtained by performing the calculation for 10^{16} incident particles in each

5. Discussion

We observed angle-dependent charge fractions of ^{16}O ions for 1.9 - 52.1 μg/cm^2 carbon targets. For thinner targets such as 1.9, 3.0 and 3.2 μg/cm^2 in thickness non-equilibrium charge state distributions were expected, while for thicker targets such as 8, 12.6, 26.1 and 52.1 μg/cm^2 in thickness the charge state equilibrium was anticipated to be already attained. For all targets we observed that the fractions of lower charge states (3+, 4+ and 5+) decreased and those of higher charge states (6+, 7+ and 8+) increased with increasing emergence angle. It is interesting to note that we observed the similar behaviors in the angular dependence of charge fractions for the thicker targets.

In fig. 5 shows the comparison of the charge state distribution measured for a 12.6 μg/cm^2 carbon target at 0° with the calculated distributions. The charge state distribution calculated with the set A cross sections predict reasonable fractions for 5+, 6+ and 7+ states but too small fractions for 3+, 4+ and 8+ states. The experimental charge state distribution was found to be reproduced very well by the computer simulation with the set B cross sections. Moreover, it was found that the set B cross sections could reproduce reasonably well the charge state distribution measured for 3.0 μg/cm^2 at 0°, where a non-equilibrium charge state distribution was expected. This fact indicates that a set of cross sections estimated in the present analysis have reasonable magnitudes.

Using the set B cross sections, we calculated charge state distributions of ^{16}O ions after passing through I - 10 μg/cm^2 carbon targets for various initial charges. In fig. 6 charge fractions of 5+ and 7+ states are shown as a function of target thickness. It can be easily seen that the charge state equilibrium was attained at the thickness of about 7 μg/cm^2. For carbon targets which are thinner than 5 μg/cm^2, charge fractions are proved to be very sensitive to ion initial charges. Using these thin targets together with incident ions of various charges, we could obtain much more detailed information on charge-changing cross sections.

In fig. 3(d) are shown angle-dependent charge fractions measured for a 52.1 μg/cm^2 carbon target, which is more than seven times thicker than 7 μg/cm^2 where the charge state equilibrium is reached. Experimental data clearly show that fractions of 4+ and 5+ states still

decrease and those of 7+ and 8+ states increase with increasing emergence angle. Hence, it is likely that angle-dependent charge fractions can be observed even for a very thick target, e.g. for a carbon target of more than 100 $\mu g/cm^2$ in thickness.

The authors would like to thank Professor K. Imai for the use of the tandem Van de Graaff accelerator and his support throughout the work. Thanks are also due to Drs. K. Takimoto and M. Nakamura and members of the Tandem Van de Graaff Laboratory of Kyoto University for their kind cooperation.

REFERENCES

1. H. D. Betz, Rev. Mod. Phys. 44 (1972) 465.
2. K. Shima, T. Mikumo and H. Tawara, At. Data Nucl. Data Tables 34 (1986) 357.
3. K. Shima, N. Kuno, M. Yamanouchi and H. Tawara, At. Data Nucl. Data Tables 51 (1992) 173.
4. R. Ishiwari, N. Shiomi and N. Sakamoto, Phys. Rev. A25 (1982) 2524.
5. G. A. Ifelov and Yu. N. Zhukova, Phys. Status Solidi B110 (1982) 653.
6. J. C. Eckardt, G. H. Lantschner, M. M. Jakas and V. H. Ponce, Nucl. Instr. Meth. B2 (1984) 168.
7. H. Gelssel, W. N. Lennard, H. R. Andrews, D. P. Jackson, I. V. Mitchell, D. Phillips and D.Ward, Nucl. Instr. Meth. BI2 (1985) 38.
8. Q. C. Kessel, Phys. Rev. A2 (1970) 1881.
9. I. Ben-Itzhak, A. Mann, M. Meron and B. Rosner, Phys. Rev. A40 (1989) 2928.
10. H. Knudsen, H. K. Haugen and P. Hvelplund, Phys. Rev. A23 (1981) 597.
11. S. A. Boman, E. M. Bernstein and J. A. Tanis, Phys. Rev. A39 (1989) 4423.
12. 0. Heber, G. Sampoll, B. B. Bandong and R. L. Watson, Phys. Rev. A40 (1989) 5601.
13. 0. Heber, G. Sampoll, R. J. Maurer, B. B. Bandong and R. L. Watson, Nucl. Instr. Meth. B40/41 (1989) 197.
14. P. Sigmund and K. B. Winterbon, Nucl. Instr. Meth. 119 (1974) 541.

Figure Captions

Fig. I : Schematic diagram of experimental setup. Scattered ^{16}O ions of various charge states are split vertically by a pair of permanent magnets and detected by a position sensitive de tector (PSD). Tile detector system, which is consisted of a vertical slit and a PSD, is movable in the horizontal plane perpendicular to the direction of the incident ^{16}O ion beam in a range of a few cm. The width of the horizontal and the vertical slits is 0.5 mm. Lengths given in the figure are in mm.

Fig. 2 : Typical position spectra taken for a carbon target of 3.0 $\mu g/cm^2$ are shown, (a): measured at 0° and (b): measured at 0.49°.

Fig. 3 : Charge fractions of 4+, 5+, 6+, 7+ and 8+ states are shown as a function of emergence angle, (a) for a 1.9 $\mu g/cm^2$ carbon target; (b) for a 8.0 $\mu g/cm^2$ carbon target; (c) for a 26.1 $\mu g/cm^2$ carbon target; and (d) for a 52.1 $\mu g/cm^2$ carbon target.

Fig. 4 : Single-electron capture cross sections calculated with the scahng law of Knudsen et al.(Ref. 10) are compared with those measured by Boman et al. for 16 MeV ^{16}O ions passing through D_2, He, Ne, Ar and Kr (Ref. 11). Symbols represent initial charge states as follows: ●5+; ▲6+; ■ 7+; ◆ 8+.

Fig. 5 : Experimental charge fractions measured at 0° for a carbon target of 12.6 $\mu g/cm^2$ are compared with the results of computer simulations. Open circles indicate the results

calculated with the set A cross sections and solid circles represent those with the set B cross sections .

Fig. 6 : Calculated charge fractions of 5+ and 7+ states, which are obtained for incident ^{16}O ions of various charge states, are shown as a function of target thickness. Symbols represent initial charge states as follows: ○ 3+; ⊙ 4+; ● 5+; □ 6+; ■ 7+; ⊕ 8+.

Table 1. The estimation methods of electron-capture and -loss cross sections used in the present simulation are shown. The meaning of symbols is given in the text.

	Set A	Set B
$\sigma_{q,q-1}$	calculated by the scaling law (Ref.10)	$\sigma_{q,q-1}$ (set A) for q=1-3,7 and 8 $\sigma_{4,3}$ (set A) x 1,8 $\sigma_{5,4}$ (set A) x1,4 $\sigma_{6,5}$ (set A) x 1,06
$\sigma_{q,q+1}$	calculated by the empirical formulas (Ref.11) for q = 5,6 and 7 N $\sigma_{5,6}$ for q = 0 - 4	$\sigma_{q,q+1}$ (set A) for q=0-5 $\sigma_{6,7}$ (set A) x 1,17 $\sigma_{7,8}$ (set A) x 3,50
$\sigma_{q,q-2}$	$\left(\frac{q}{8}\right)^6 \sigma_{8,7}\ x\ 0{,}15$	$\sigma_{q,q-2}$ (set A)
$\sigma_{q,q+2}$	$\frac{N(N-1)}{12}\sigma_{2,3}\ x\ 0{,}40$ for q = 0 - 4 $\sigma_{5,7} = 0{,}10x\ \sigma_{4,6}$ $\sigma_{6,8} = 0{,}01x\ \sigma_{4,6}$	$\sigma_{q,q+2}$ (set A)

Experimental Setup

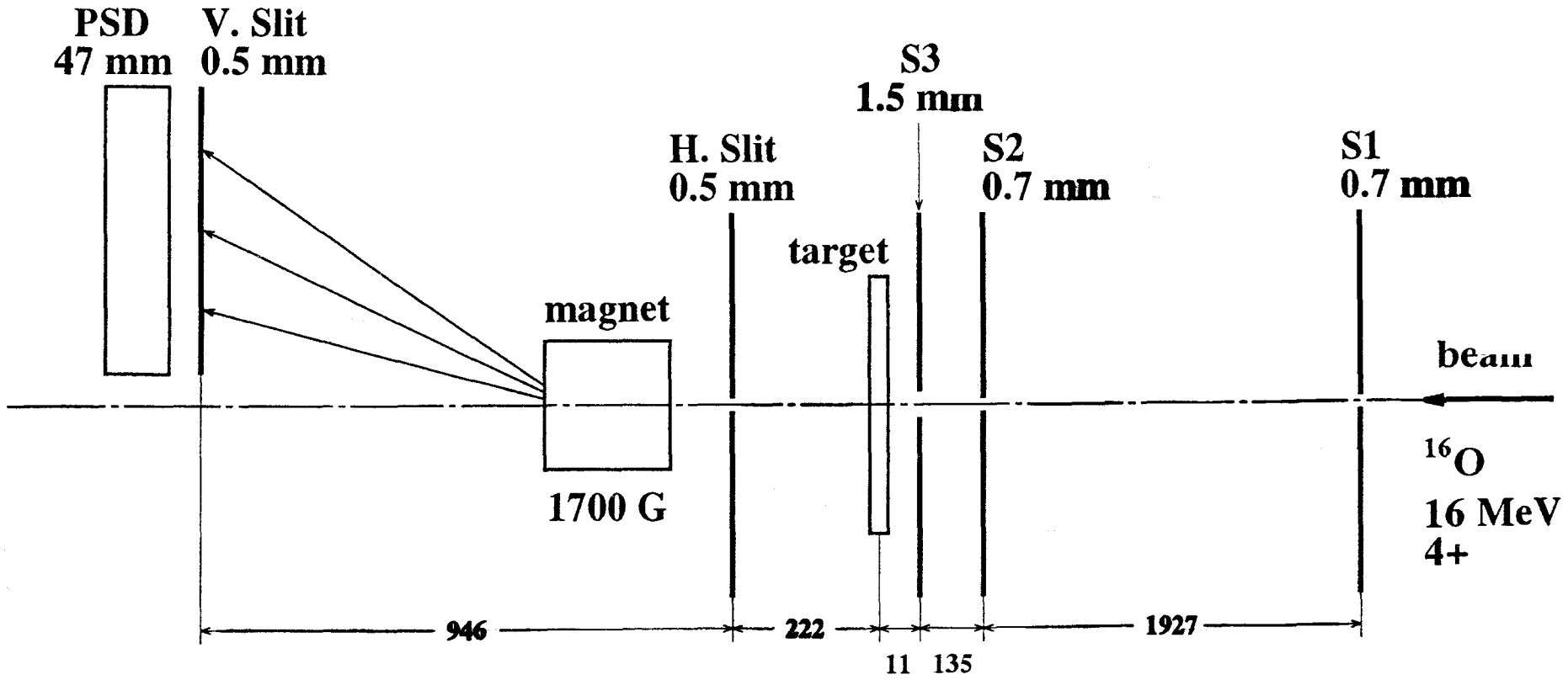

Fig.1

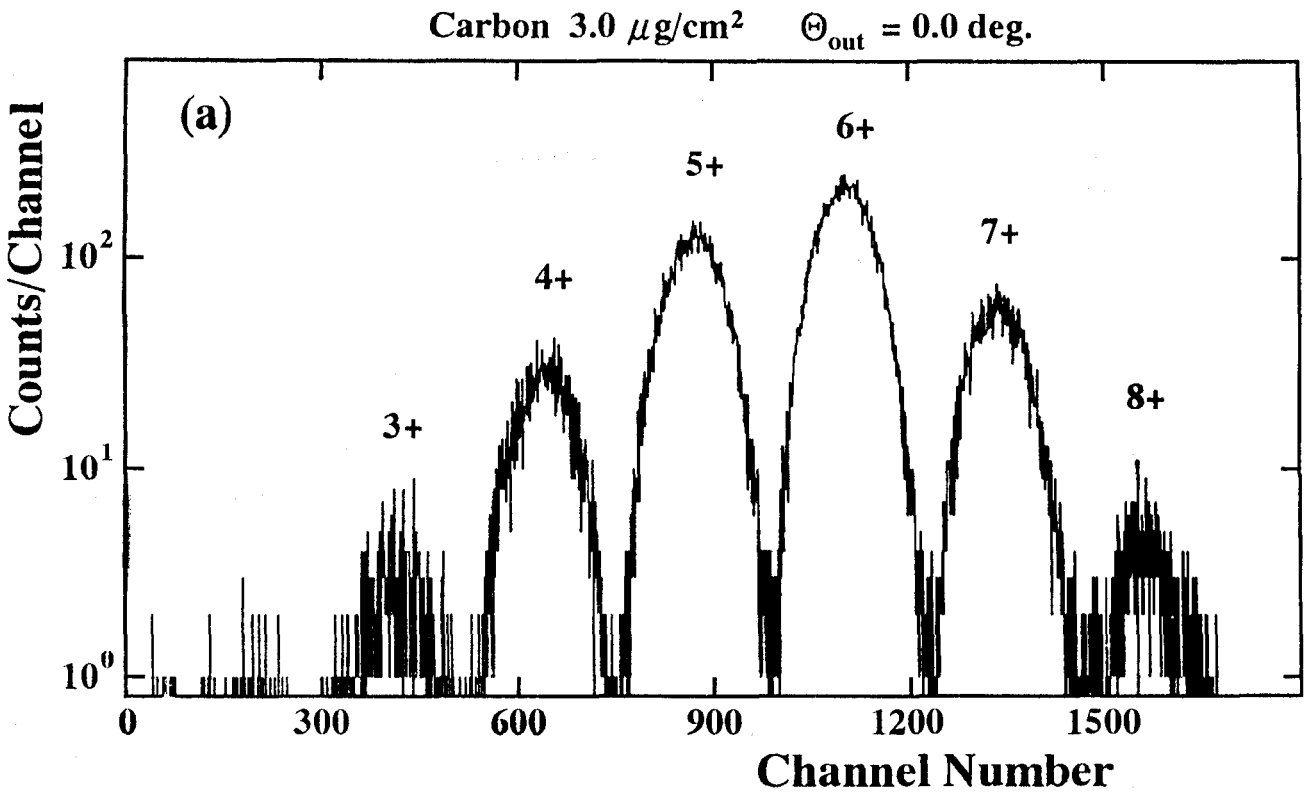
Carbon 3.0 μg/cm² Θout = 0.0 deg.
(a)
Counts/Channel
10²
10¹
10⁰
3+
4+
5+
6+
7+
8+
0
300
600
900
1200
1500
Channel Number

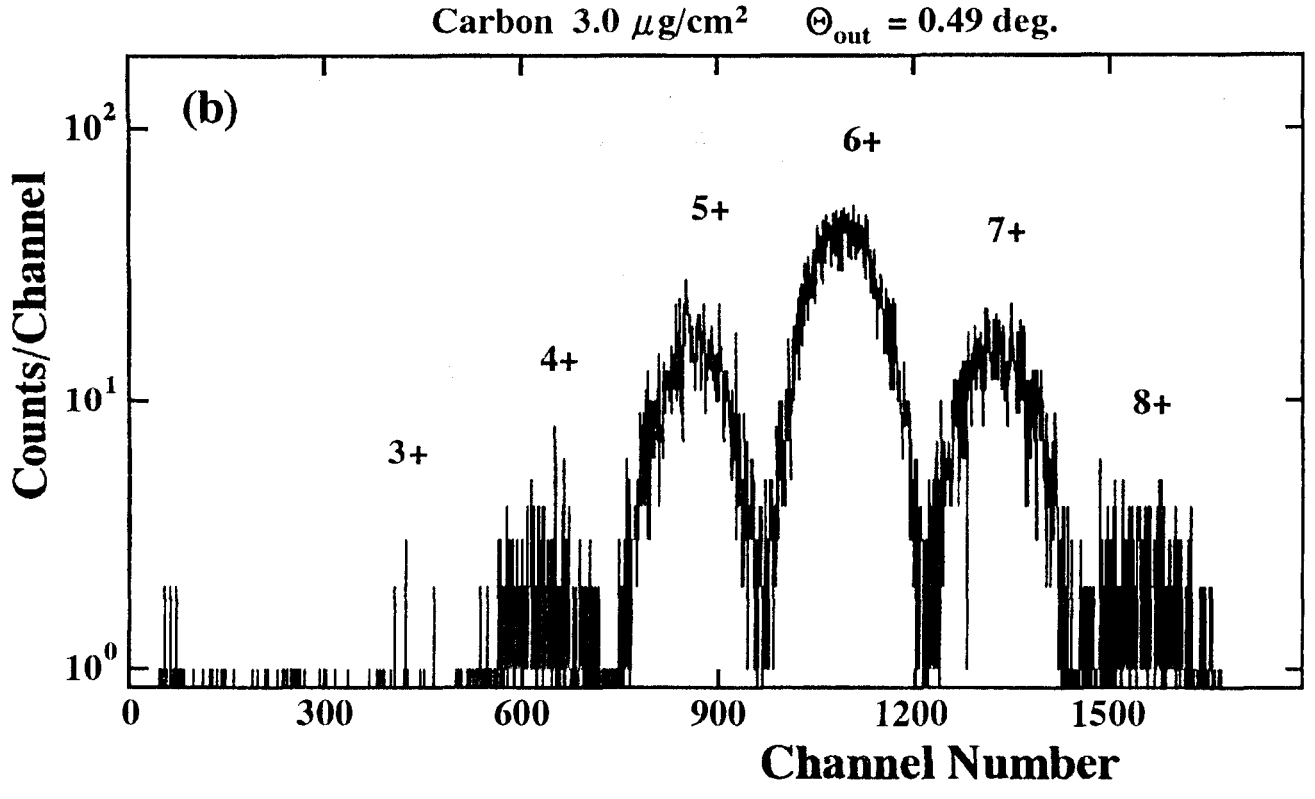
Carbon 3.0 μg/cm² Θout = 0.49 deg.
(b)
Counts/Channel
10²
10¹
10⁰
3+
4+
5+
6+
7+
8+
0
300
600
900
1200
1500
Channel Number

Fig.2

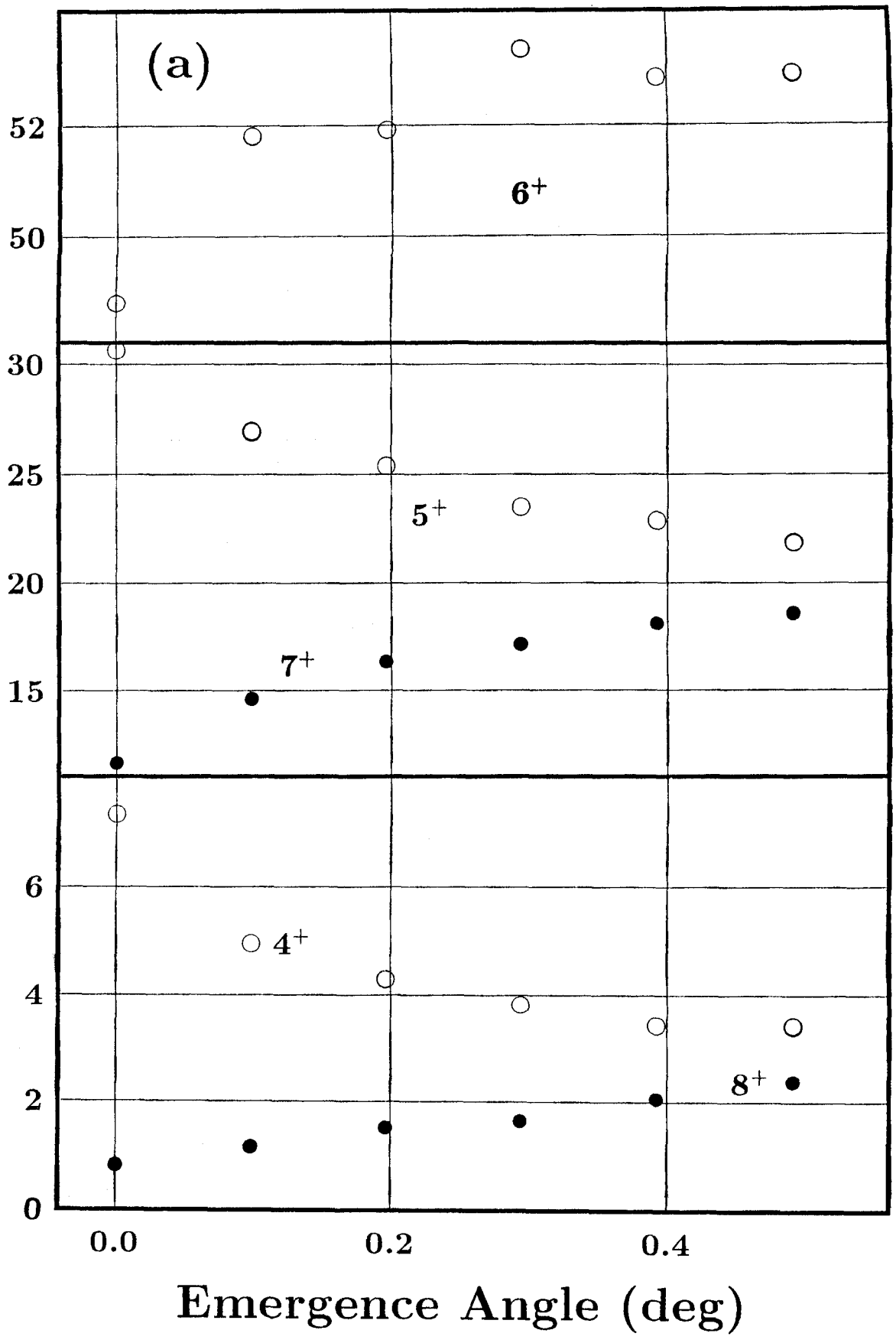
Charge Fraction (%)
Carbon 1.9 μg/cm²
(a)
52
50
30
25
20
15
6
4
2
0
6+
5+
7+
4+
8+
0.0
0.2
0.4
Emergence Angle (deg)

Fig.3a

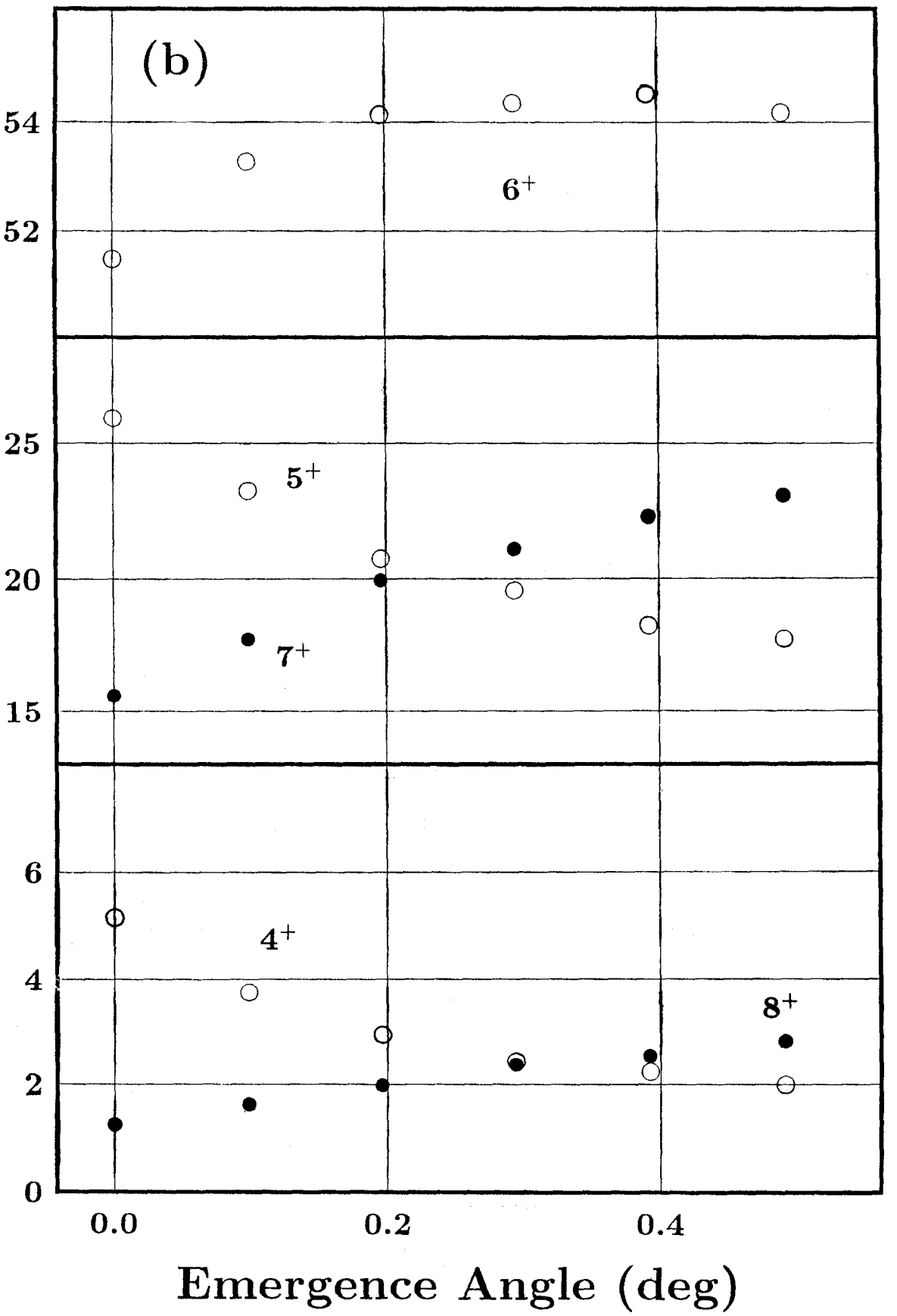
Charge Fraction (%)
Carbon 8.0 μg/cm²
(b)
54
52
25
20
15
6
4
2
0
6+
5+
7+
4+
8+
0.0
0.2
0.4
Emergence Angle (deg)

Fig.3b

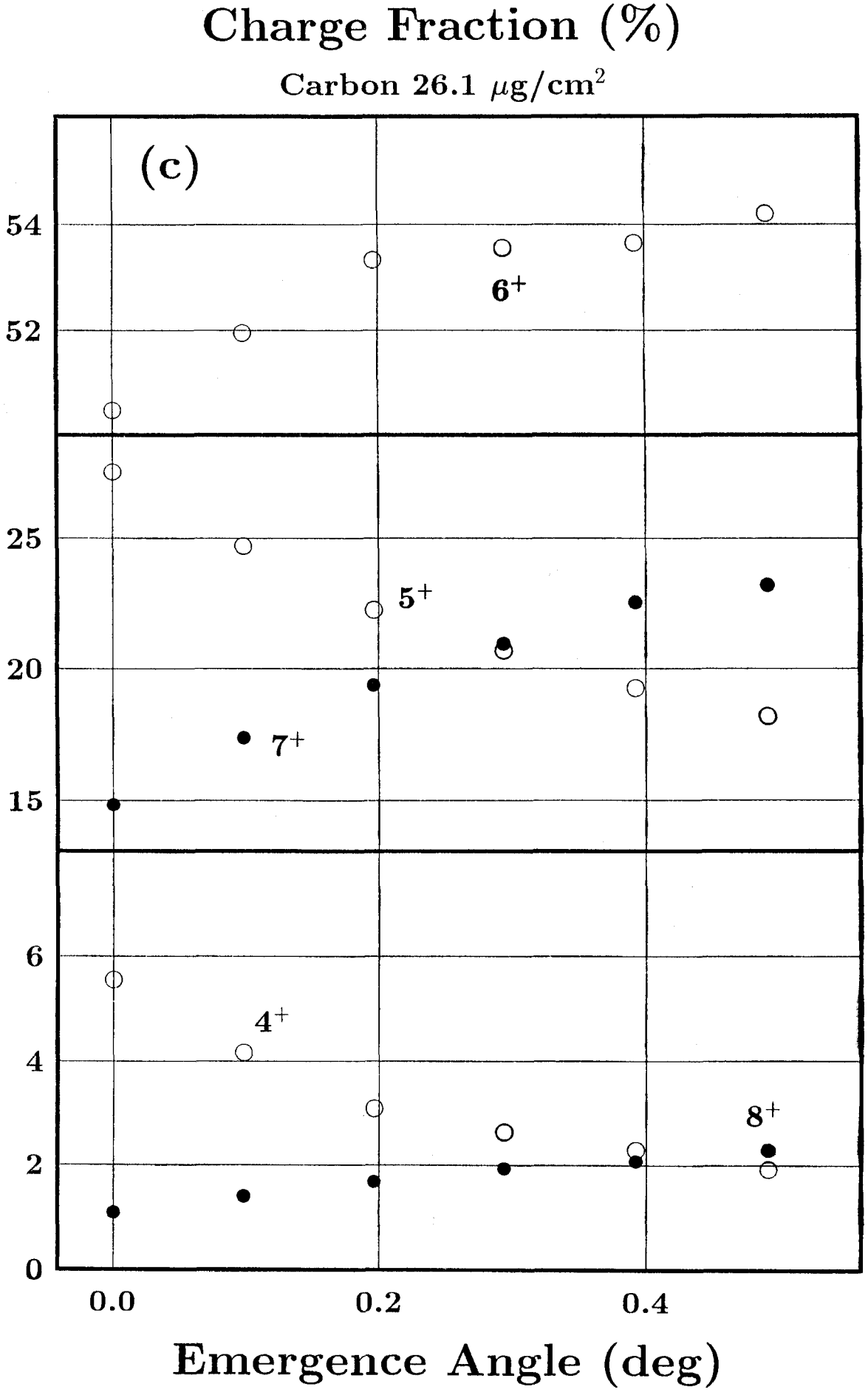
Charge Fraction (%)
Carbon 26.1 μg/cm²
(c)
54
52
25
20
15
6
4
2
0
6+
5+
7+
4+
8+
0.0
0.2
0.4
Emergence Angle (deg)

Fig.3c

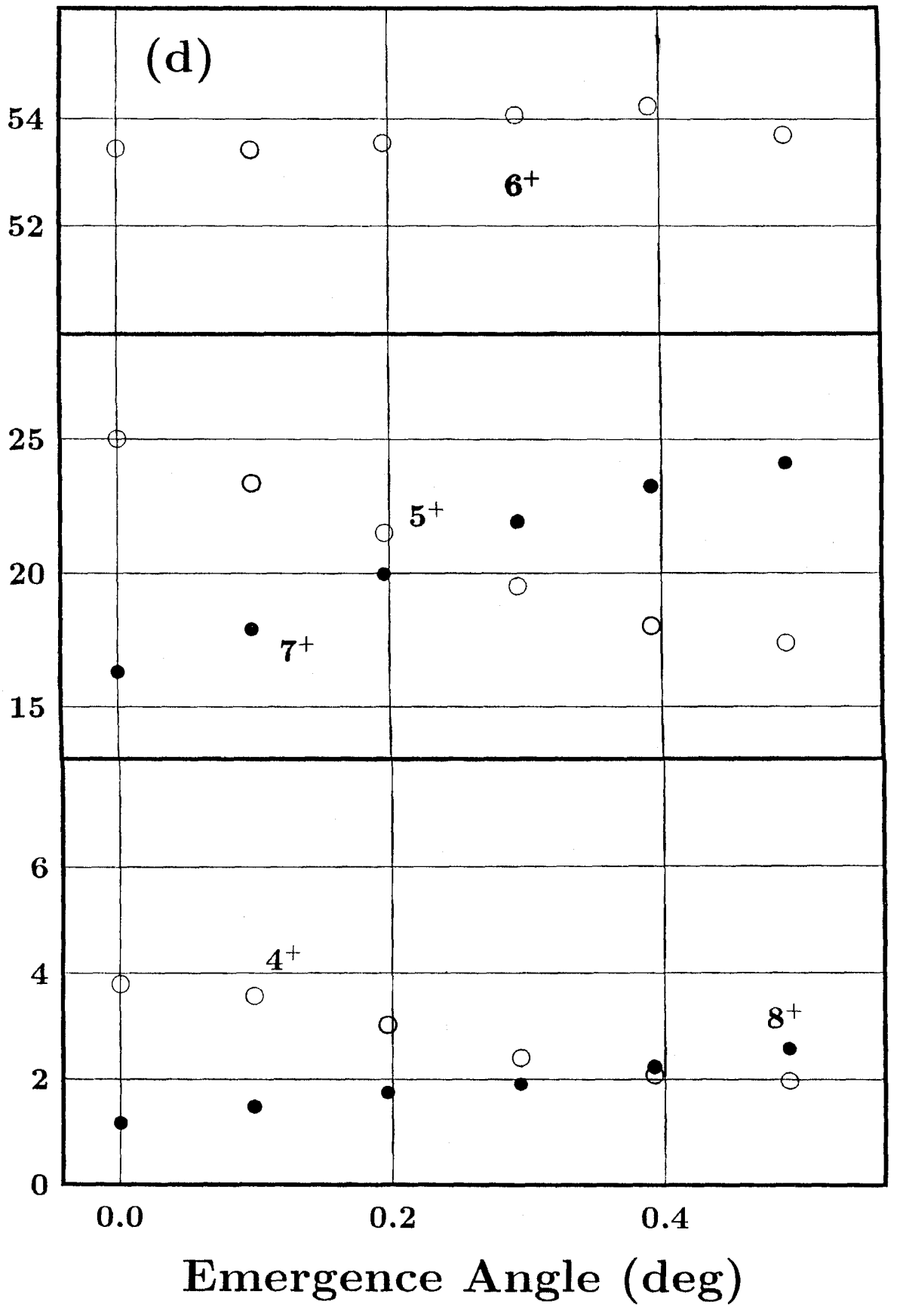
Charge Fraction (%)
Carbon 52.1 μg/cm²
(d)
54
52
25
20
15
6
4
2
0
6+
5+
7+
4+
8+
0.0
0.2
0.4
Emergence Angle (deg)

Fig.3d

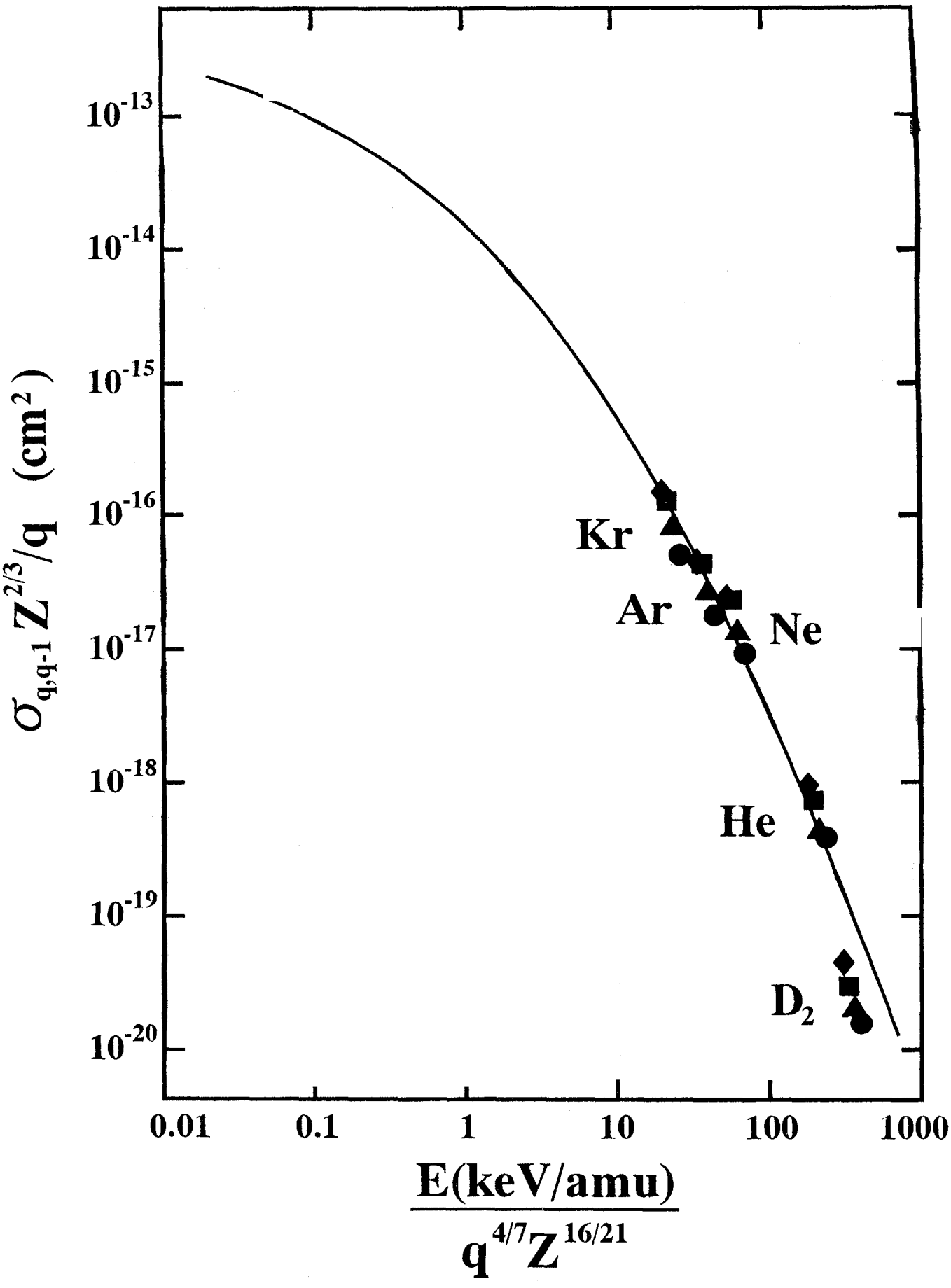
10^{-13}
10^{-14}
10^{-15}
10^{-16}
10^{-17}
10^{-18}
10^{-19}
10^{-20}
$\sigma_{q,q-1} Z^{2/3}/q$ (cm^2)
Kr
Ar
Ne
He
D_2
0.01
0.1
1
10
100
1000
$\frac{E(keV/amu)}{q^{4/7} Z^{16/21}}$

Fig.4

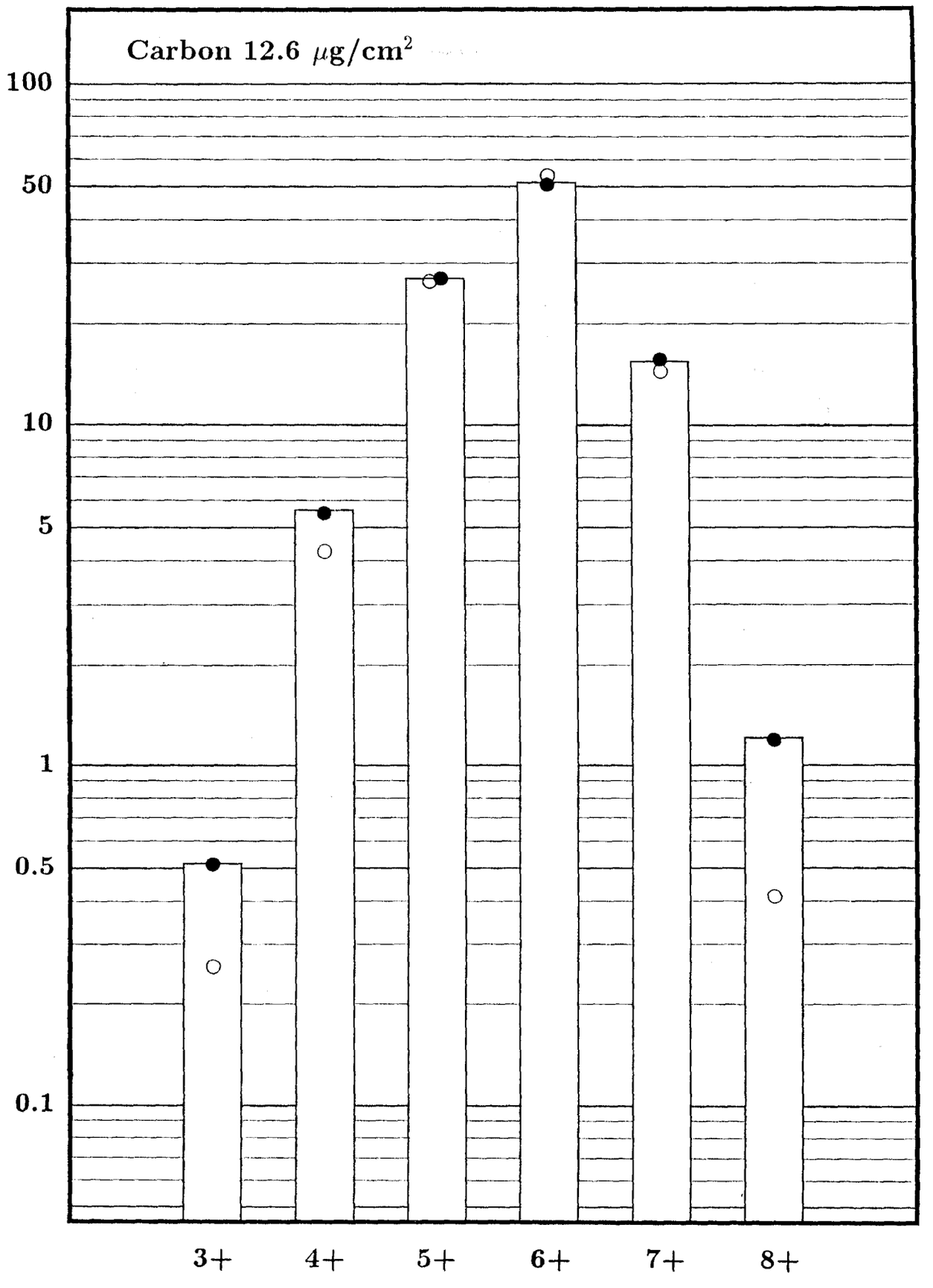

Fig.5

Charge Fraction (%)